Transportation Geotechnics 55 (2025) 101706

Contents lists available at ScienceDirect

Transportation Geotechnics

journal homepage: www.elsevier.com/locate/trgeo

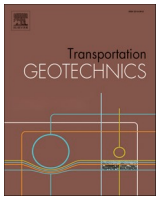

Development and application of the Illinois Buckle Risk Model (IBRM) using multi-source track condition data

Neeraj Thakur [a], Arthur de O. Lima [a], Marcus S. Dersch [a], J.Riley Edwards [a,*]

[a] Rail Transportation and Engineering Center – RailTEC, Department of Civil and Environmental Engineering, The Grainger College of Engineering, University of Illinois at Urbana-Champaign, Newmark Civil Engineering Laboratory, MC-250, 205 N. Mathews Ave., Urbana, IL 61801, USA

ARTICLE INFO

Keywords:
Track buckles
Track lateral strength
Sun kink
Buckle risk
Track maintenance prioritization

ABSTRACT

Track buckles occur more frequently in Continuously Welded Rail (CWR) as they lack joints to accommodate axial thermal expansion. Analysis of Federal Railroad Administration (FRA) accident database reveals that buckled-track derailments have been a persistent safety concern for U.S. railroads. The FRA initiated an extensive research program in the 1980's to develop and experimentally verify a dynamic buckling theory which culminated in the development of the CWR-SAFE software. The Buckle module of CWR-SAFE accepts quantitative track condition input parameters and assesses the buckling risk of track in terms of its Buckling Safety Margin (BSM). BSM is a composite metric that accounts for track strength, rail temperature, and rail neutral temperature.

Since the development of CWR-SAFE, there have been notable advancements in track inspection technologies capable of providing high-resolution track health data. The Illinois Buckle Risk Model (IBRM) leverages the outputs from three-dimensional machine vision and track geometry measurements systems into the CWR-SAFE environment to perform buckle risk assessment at an individual crosstie resolution. IBRM uses results from field and laboratory experiments to calibrate inspection system outputs into quantified inputs for CWR-SAFE. The application of IBRM is demonstrated using data collected from a Class I railroad subdivision. BSM calculations show that 1.9% of the subdivision track is in the desired range, 95.7% is in the adequate range, and 2.4% is in the minimum required range. This information can be used to prioritize both capital renewal projects and maintenance interventions. Results also demonstrate the IBRM's flexibility and scalability for buckle risk assessment.

Introduction and Background

The need for higher operational speeds and reduced track maintenance costs led the railroads to adopt Continuously Welded Rail (CWR) as a replacement for conventional jointed track[1]. Despite CWR's many advantages, a major drawback is its higher propensity to buckle compared to jointed track. CWR does not have joints that facilitate expansion due to changes in rail temperature thus compressive axial forces are generated that can result in lateral track buckles[1]. Track buckles have been a concern for high speed and heavy tonnage rail corridors since 1960, a date that correlates with more widespread adoption of CWR[2,3]. A review of the Federal Railroad Administration (FRA) train accident data reveals that buckled-track derailments occur at a higher-than-average frequency and result in more severe derailments than other track-caused accidents[4]. Between 2015 and 2024, there were 80 track-buckle-caused derailments on U.S. Class I railroad mainlines, resulting in approximately $101 million USD in damages[5].

Track buckling theory

The possibility of track buckling in jointless track appeared in engineering literature as early as 1902[1]. Experimental research on buckling and theories to analyze the buckling phenomenon were proposed starting in the early 1930's. In 1975, Kerr [1] published a survey that provided a comprehensive overview of the existing research and developments in lateral track buckling up to that time. Kerr summarized the strengths and limitations of the test setups and the corresponding theories and proposed assumptions for a more consistent analytical framework. Based on these assumptions, Kerr [6] divided the track into three regions (i.e., buckled, adjoining, and infinite) and used variational calculus to obtain differential equations for the buckled region (Fig. 1).

* Corresponding author.
E-mail addresses: neerajt2@illinois.edu (N. Thakur), aolima@illinois.edu (A.O. Lima), mdersch2@illinois.edu (M.S. Dersch), jedward2@illinois.edu (J.Riley Edwards).

https://doi.org/10.1016/j.trgeo.2025.101706
Received 18 April 2025; Received in revised form 8 August 2025; Accepted 1 September 2025
Available online 4 September 2025
2214-3912/© 2025 The Author(s). Published by Elsevier Ltd. This is an open access article under the CC BY-NC-ND license (http://creativecommons.org/licenses/by-nc-nd/4.0/).

The safe rail temperature was calculated for track constructed with 115 RE rail on timber crossties with cut spike fasteners. Samavedam [7] advanced this research by incorporating the full nonlinear behavior of the longitudinal stiffness in the adjoining regions. This line of research was further advanced through experimental verification, incorporation of additional parameters, and extensive laboratory and field testing that will be described in Section 1.2 [8,9,10,11]. While this research primarily leverages results from these works, other researchers have contributed to advancing the understanding of track buckling mechanics [12,13,14,15,16,17,18]. Additionally, researchers have used multibody dynamic models[19]and incorporated dynamic forces in finite element models[20]for buckle risk assessment.

Early track buckle modeling and validation

In 1978, the FRA initiated a major research program that was managed by the Transportation System Center (now John A. Volpe National Transportation Systems Center) to reduce the number of track buckles[21]. The aim of this research was to develop safety recommendations to prevent buckle-caused derailments. In 1982, an analytical framework was proposed to explain the mechanism of track buckling under static conditions[21]. The theory accounted for various influencing factors, including rail properties, lateral resistance, longitudinal stiffness, initial misalignment, and Rail Neutral Temperature (RNT). To validate the analysis, two revenue service tests were conducted on tangent and curved track on the Southern Railway (now part of Norfolk Southern Railway). While the theoretical predictions showed good agreement with the experimental results, the study's authors recommended dynamic buckling tests to evaluate the effects of rail liftoff and the consequent reduction in lateral resistance[21].

As a result, dynamic buckling theory was introduced in 1985 to describe the influence of moving vehicles on track stability[9]. This analysis incorporated additional parameters such as vehicle configuration, vertical stiffness, and the crosstie-ballast friction coefficient. Theoretical calculations for tangent track sections indicated a marked reduction in dynamic buckling critical temperature under long railcars when compared to the static buckling temperatures obtained in earlier studies. Experimental analyses were subsequently conducted to validate the theoretical predictions of dynamic buckling and demonstrated good agreement with the theoretical results[22]. Furthermore, the researchers recommended investigations to better characterize track lateral resistance by quantifying the individual contributions of key components, including the shoulder, crib, and support ballast sections [22].

Lateral resistance quantification

Two common methods for evaluating the lateral strength of track are the Single Tie Push Test (STPT) and the Track Lateral Pull Test (TLPT). TLPTs assess lateral track resistance by mobilizing an entire section of track, thereby providing a comprehensive measure of the track's lateral stability. In contrast, STPTs quantify the lateral resistance at an individual crosstie by applying a lateral force and measuring its load–deflection behavior. Notably, STPT is a non-destructive, minimally invasive test that can be conducted using portable equipment. STPTs offers practical advantages over TLPTs, particularly in field conditions where minimizing disruption to track operations is essential. Empirical studies have demonstrated that average values obtained from multiple STPTs can be translated into equivalent TLPT measurements by modeling the rail as an infinitely long beam supported on a non-linear elastic foundation[10].

The STPT yields three measurements that characterize the lateral resistance of the track: peak resistance, limit resistance, and the displacement interval between the peak and limit resistance. Field experiments were conducted to establish an empirical relation between peak and limit resistance with the intention of reducing testing-induced track disturbance[10]. This relation ensured that a single measurement of peak resistance would suffice to quantify the lateral strength of ballast. A total of 1,377 STPTs and 40 TLPTs were conducted between 1985 and 1989 to characterize lateral resistance. These tests were conducted to isolate the effects of various components of ballast (crib, shoulder, and support) as well as ballast type and consolidation, track curvature, loading methodology, and loading rate[10].

Longitudinal and torsional resistance quantification

Samavedam et al. [11] evaluated track longitudinal resistance through tests conducted at the Transportation Technology Center (TTC) in Pueblo, Colorado. A total of nine tests were performed on crosstie panels that were isolated from the remainder of the track structure. These tests were conducted under a variety of anchorage patterns and ballast conditions. Additionally, the researchers carried out two series of tests to quantify the torsional resistance provided by common rail fastening systems. The first series was conducted under controlled laboratory conditions, while the second series assessed the in-situ response under field conditions.

CWR-SAFE

Results from the FRA-funded track buckle research described above culminated in the development of the CWR-SAFE software package[23]. CWR-SAFE was developed as a simple platform that allows users to input categorical and quantitative track parameters to obtain a quantifiable output for buckle risk. There are three modules within CWR-SAFE: Indy, Buckle, and Risk. The Buckle module is considered the computation engine of the software package which performs the numerical evaluation of buckle strength based on deterministic quantitative inputs[8].

Track parameters including lateral resistance, longitudinal stiffness, torsional resistance, rail size, crosstie and ballast properties, lateral misalignment amplitude, vehicle configuration, and track vertical stiffness are input into the Buckle module to calculate the upper and lower critical buckling temperatures. The lower critical temperature refers to the temperature at which track buckle occurs in the presence of an external disturbance, such as train loading. In contrast, the upper critical temperature is the threshold at which track is expected to buckle without any external energy input. Based on the difference between the upper and lower critical temperatures, the software applies a track quality-based safety criterion to determine the allowable temperature increase ($\Delta T_{allowable}$). $\Delta T_{allowable}$ represents a quantifiable measure of track strength, expressed in terms of temperature. The resulting output is next used by the software to calculate the track's Buckling Safety Margin (BSM) using Equation (1):

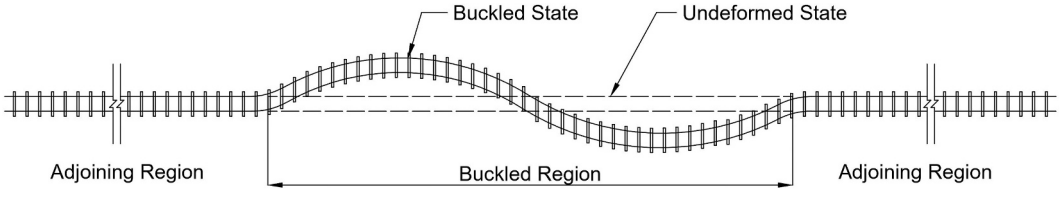

Fig. 1. Schematic showing buckled and adjoining region (Adapted from [6]).

$$BSM = \Delta T_{allowable} - (T_{rail} - RNT) \quad (1)$$

Where RNT represents the temperature at which the rail has no axial stress (also known as the Stress-Free Temperature) and T_{rail} is the rail temperature which indicates the thermal stress in the rail. BSM is a useful quantitative metric that establishes the reserve track strength available to resist buckling [8,24,25]. Zarembski et al. [26] developed an empirical method to assess buckle risk using factors derived from CWR-SAFE, Kerr's buckling theory [6], longitudinal creep theory, and expert evaluation.

The CWR-SAFE Indy module was developed to perform quick assessments of track strength by railroad industry practitioners. Indy accepts qualitative inputs that are internally converted into numeric values. Conversions are performed using the empirical correlations developed from the track resistance characterization tests described earlier.

The CWR-SAFE Risk module accepts probabilistic input parameters to evaluate the expected number of track buckles per year for a given track segment with a known annual temperature profile. To account for the inherent uncertainty in track conditions, the module incorporates probabilistic distributions for the three most sensitive – and often highly variable – track parameters influencing track buckling strength: RNT, lateral misalignment, and lateral resistance. Many researchers have attempted to develop non-destructive and reference-free methods for accurately quantifying RNT[27,28,29,30,31,32]. Presently there are no known moving platform systems that can collect such data, with VERSE being the most common method used to obtain RNT for revenue service track[33]. Meanwhile, there have been major advancements in track inspection systems that can now provide highly granular data for track conditions and health parameters that can be used to enhance the accuracy and precision of buckling risk assessment.

Evolution in track inspection systems and data

Track geometry refers broadly to the geometric position and condition of railroads curves and tangents with respect to their intended design, use, and maintenance[34]. One of the primary forms of railroad regulatory oversight provided by the FRA is its jurisdiction over track geometry thresholds that must be met for a given track class and associated maximum train allowable train speed. Geometry thresholds are maintained by the FRA in the Code of Federal Regulations (CFR) Part 213, the Track Safety Standards[35]. Traditionally, these measurements were captured by hand at specific locations. This was followed by the development and deployment of track geometry cars or trainsets that are operated by humans that serve as continuous means for data collection as they travel along the track.

The next major advancement in track geometry quantification and data collection came through the development of unattended systems such as the Autonomous Track Geometry Measurement System (ATGMS) which began in 2006 with demonstrations in freight service by 2017[36,37,38]. These systems are railcar-based non-contact measurement systems that typically use inertial and optical measurement principles to measure track geometry parameters such as gauge, profile, alignment, cross level and curvature[37]. ATGMS collects track data automatically with minimal human intervention and are commonly deployed on revenue service trains which allows geometry data collection at increased frequencies. These data can be transferred to a central server through commercial communication services for a near real-time assessment of track geometry at a foot-by-foot interval. Class I railroads have deployed this technology in revenue service for the collection of track geometry data at frequencies higher than those mandated by the FRA in CFR 213[39].

The use of machine vision for railroad track inspection started in the early 2000's and has seen significant improvements since then. Machine vision has been used to detect irregularities and defects in timber crossties fasteners, rail anchors, crib ballast, and turnout components [40,41]. Additionally, several researchers have used machine vision technology for real-time monitoring of track health[42,43,44]. In a comprehensive review, Aela et al. [45] identified different vision-based methods for railroad infrastructure monitoring and inspection: Digital Image Correlation (DIC), Light Detection and Ranging (LiDAR), thermal imaging, X-ray Computed Tomography (CT), and robots. LiDAR and machine vision can be coupled for determining ballast cross section, crosstie type, and potentially the shape of ballast particles [46]. The most popular methods for image classification are Support Vector Machines (SVM), Decision Trees, K Nearest Neighbor (KNN), Artificial Neural Networks (ANN), and Convolutional Neural Networks (CNN) [47]. CNN based deep-learning methods have outperformed traditional algorithms in machine vision applications[48].

LR*AI*L is a rail inspection system based on the principle of laser triangulation and combines high-power, invisible, laser line projectors, and synchronized cameras to capture high-resolution-intensity images and 3-dimensional (3D) range profile of track[49]. LR*AI*L uses both traditional algorithms and Deep Convolutional Neural Networks (DCNNs) for image recognition, characterization of component conditions, and measurement of key track features. Field tests have demonstrated LR*AI*L's accuracy for assessing fasteners and spikes[50,49]; [51]).

Objective

The novel objective of this research is to combine detailed geometry data with track component data into the Illinois Buckle Risk Model (IBRM) by leveraging the CWR-SAFE calculation environment. The IBRM will be used to identify locations with high buckling susceptibility for timely, prioritized maintenance interventions.

Methodology

This research uses track condition and heath data from two primary sources: geometry measurements from ATGMS and track component data from LR*AI*L. ATGMS provides processed track geometry space curve data output as chordal measurements at one-foot intervals. Raw LR*AI*L data is converted from millimeter (or sub-mm) resolution to component-level outputs on a tie-by-tie basis. LR*AI*L data corresponding to a crosstie and the surrounding cribs are then calibrated and converted into quantifiable values based on findings from previous field and laboratory experiments.

Data preparation

Before further analysis, the geometry and component data streams must be spatially aligned for a single inspection campaign and between consecutive runs. The geometry data used in this research is pre-aligned and included mileposts assignments provided by a third-party vendor, whereas the LR*AI*L data contained only GPS coordinates. For this research the data are aligned using a k-dimensional (k-d) tree algorithm to efficiently compare GPS coordinates from both data sources to identify the closest matches for accurate spatial alignment[52]. The k-d tree algorithm organizes points in a k-d space for efficient nearest-neighbor searches and recursively partitions points along axes, balancing the tree for optimal performance[53].

CWR-SAFE

Next, the CWR-SAFE Buckle module is used to evaluate the BSM for individual crossties based on appropriate values for required input parameters (Table 1).

The CWR-Safe Buckle module executes analytical calculations based on deterministic input parameters to estimate $\Delta T_{allowable}$. The BSM is computed using Equation (1) to account for rail temperature and RNT. Defined ranges for BSM values from the literature are summarized in Table 2 [8]along with their color designation for visualization on maps

Table 1
CWR-SAFE Buckle module input parameters.

Track Parameters	Unit	Range of Inputs
Rail size	lbs/ft	AREA / AREMA – 100, 115, 119, 132, 133, 136, 140, UIC – 54, 60, and user defined
Crosstie type		Wood, Concrete
Ballast type		Granite, Slag, User-Defined
Crosstie lateral force (peak resistance)	lbs/in (kN/mm)	50 – 300 (8.7 – 52.5)
Crosstie weight	lbs (kN)	150 – 1,000 (0.7 – 4.5)
Crosstie spacing	in (mm)	12 – 36 (305 – 914)
Track curvature	Degrees (Radius in m)	0 – 15 (∞ – 117)
Crosstie ballast friction coefficient		0.65 – 2.3
Torsional resistance	in-kips/rad/in (m-kN/rad/m)	0 – 500 (0 – 2,224)
Longitudinal stiffness	psi (kPa)	25 – 500 (172 – 3,447)
Foundation modulus	psi (MPa)	2,000 – 10,000 (13.8 – 68.9)
Misalignment amplitude	in (mm)	0.1 – 3.0 (2.5 – 76.2)
Misalignment half – wavelength	in (m)	75 – 500 (1.9 – 12.7)
Vehicle Type		Box car, Hopper, Locomotive, Tank car, User-Defined

Table 2
Buckling Safety Margin (BSM) ranges and color assignments.

Range	BSM Values	Color
Desired	> 40 ℉ (4.4 ℃)	Green
Adequate	20 to 40 ℉ (−6.7 to 4.4 ℃)	Yellow
Minimum Required	0 to 20 ℉ (−17.8 to −6.7 ℃)	Red
No margin	< 0 ℉ (< −17.8 ℃)	Black

and charts.

Component data from LRAIL

Lateral resistance quantification

The lateral resistance of the track is influenced by many factors including the type of crosstie, crosstie-ballast friction coefficient, volume and shape characteristics of the ballast and its cross section, degree of ballast consolidation, and ballast maintenance interventions that influence consolidation[54]. STPT tests were conducted for various combinations of these factors[10]and their results can be integrated with outputs from LRAIL to estimate the lateral strength. Specifically, LRAIL can identify the type of crosstie and provide information on ballast volume at 1-meter intervals. LRAIL defines a horizontal reference plane at the top of the rail from which all ballast profile measurements are referenced.

To correlate experimental results to LRAIL track condition data and quantify the influence of ballast cross section on track strength we developed two metrics: shoulder effectiveness and crib effectiveness (Fig. 2). Lines and hatch patterns represent actual (blue) and design (red) ballast cross-sections (Fig. 2). Shoulder effectiveness (E_s) is the proportion of the actual shoulder area of the ballast within the defined design cross-sectional area, expressed as a percentage. This effectiveness is computed separately for the left and right shoulders, with the lower of the two values selected given the track would likely buckle toward the weakest side. Crib effectiveness (E_c) is calculated by determining the ratio of the actual ballast height within the crib area to the design height (i.e., full crib). The maximum achievable effectiveness for both values is capped at 100 %. The shoulder effectiveness for the subdivision described in this research ranges from 0 % to 99.9 % whereas the crib effectiveness ranges from 43.1 % to 99.9 %. Empirical relationships derived from STPTs indicate that the average peak lateral strength for fully consolidated timber-crosstie track with 12-inch (30 cm) shoulders and full crib ballast is approximately 114 lbs/in (20 kN/m) [8]. Further, these STPTs quantified the average incremental contribution of individual ballast components to the total lateral strength[54,10], thus enabling quantification of each component's individual contribution to the overall lateral track resistance (Table 3).

For an individual crosstie (i), the lateral strength contributions of its ballast components are adjusted based on their respective ballast volumes. Specifically, the shoulder and crib effectiveness values are multiplied by their corresponding component strengths and then combined with the support ballast strength to determine the total lateral strength of the crosstie (Equation (2)).

$$F_i = (F_s \times E_{si}) + (F_c \times E_{ci}) + (F_b) \quad (2)$$

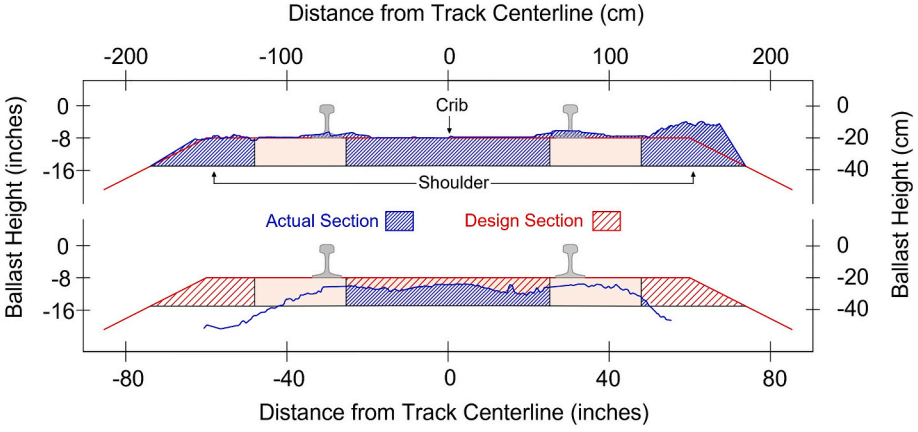

Fig. 2. Example track cross sections showing adequate (top) and inadequate (bottom). Ballast volumes. Shoulder and crib effectiveness contribution areas also identified (top)

Table 3
Ballast section component contribution to lateral strength for a fully consolidated timber-crosstie track with 12-inch shoulders and full crib ballast.

Ballast Component	Percent Contribution	Lateral Strength Contribution *lbs/in (kN/m)*
Shoulder (F_s)	25 %	28 (4.9)
Crib (F_c)	35 %	40 (7.0)
Support (F_b)	40 %	46 (8.1)
Total (F)	100 %	114 (20.0)

Two example crosstie sections at different locations representing adequate and inadequate ballast conditions are presented (Fig. 2) along with their corresponding calculations for total lateral strength (Table 4).

Longitudinal stiffness and torsional resistance quantification

The longitudinal stiffness of the track is influenced by the anchorage pattern, while torsional resistance is primarily related to the fastening system type and condition as quantified by laboratory and field tests [11]. LR*AI*L outputs include the number of anchors and the type of fasteners on a tie-by-tie level. To determine the average anchorage pattern for a region of track, the number of anchors on 30 consecutive crossties is calculated. Table 5 shows the longitudinal stiffness of track based on the anchoring pattern and the torsional resistance for different types of fastening systems used in wooden crosstie track [8].

Geometry data from ATGMS

The horizontal misalignment amplitude and degree of horizontal curve are obtained from ATGMS, with 31-foot chord alignment measurements used to detect deviations. Like other applications using track geometry data, left and right misalignment values are averaged.

Rail temperature

Rail temperature is used to determine the thermal stresses present in the rail to complete the BSM calculation. Estimated rail temperature data is obtained from ENSCO's Predictive Rail Temperature System[55] which uses a model to forecast rail temperatures using weather data and material properties. The model's calculations are based on the principles of heat transfer and account for the sun's energy absorbed by the rails as well as the energy lost through convection and radiation. Weather forecast inputs are obtained from the National Weather Service (NWS) and additional parameters such as solar radiation intensity, solar angle, wind speed, sky temperature, and the rail's heat absorptivity and emissivity are also considered. Rail temperatures are predicted across a square grid with a side length of 5.6 mi (9.0 km). The maximum annual rail temperature predicted for the track section considered in this research was 140 °F (60.0 °C).

Table 4
Total lateral strength calculation.

Parameter	Adequate Section		Inadequate Section	
Shoulder Effectiveness	98%		0%	
Shoulder Strength	0.98 x 28 lbs/in = 98 %	28 lbs/in (4.9 kN/m)	0.00 x 28 lbs/in = 72 %	0 lbs/in (0 kN/m)
Crib Effectiveness				
Crib Strength	0.98 x 40 lbs/in =	39 lbs/in (6.8 kN/m)	0.72 x 40 lbs/in =	29 lbs/in (5.0 kN/m)
Support Strength		46 lbs/in (8.1 kN/m)		46 lbs/in (8.1 kN/m)
Total Lateral Strength		113 lbs/in (19.8 kN/m)		75 lbs/in (13.1 kN/m)

Table 5
Longitudinal stiffness and torsional resistance values for different anchoring pattern and fastening systems.

Anchoring pattern/ Fastening system	Longitudinal stiffness/ Torsional resistance
Every Tie Anchored (ETA)	400 psi (2,758 kPa)
Every Other Tie Anchored (EOTA)	200 psi (1,379 kPa)
Cut spikes	80 in-kips/rad/in (356 m-kN/rad/m)
Elastic fasteners	370 in-kips/rad/in (1,646 m-kN/rad/m)

Assumptions

The type of ballast can be identified from the railroad inventory or visual inspection. The friction coefficient for crosstie-ballast interface was assumed to be 1.2 for timber crossties with granite ballast. The foundation modulus is assumed to be a constant value of 3,000 psi (20.7 MPa) for timber crosstie track[34].

The desired RNT is specified by the railroad as the preferred rail laying temperature. The actual RNT is influenced by how well the initial RNT was established, and subsequent longitudinal movement of rail, lateral shift of track, and vertical settlement of track[56]. In the U.S., CWR is typically installed with RNT ranging from 90-110 °F (32.2–43.3 °C) but this value is known to reduce to as low as 50–70 °F (10–21.1 °C) over time through the mechanisms described above[23]. For the track segment considered in the research, the preferred rail laying temperature is 105 °F (40.6 °C) and we assume it has been reduced to a RNT of 80 °F (26.7 °C).

The lateral strength of the track is reduced by the vertical lift-off of the rails between the wheels that is caused by the elastic effect of the track and its beam on elastic foundation (BOEF) behavior[57]. Vertical lift-off is most pronounced for hopper cars given their truck spacing and maximum gross rail load (GRL), making them the most critical case for BSM calculation hence their consideration in this research. The values for axle load, truck center spacing, and axle spacing used in this research are 71,500 lbs (318 kN), 664 in. (1,687 cm), and 70 in. (178 cm), respectively. The flowchart (Fig. 3) summarizes the track data sources and assumptions made in the implementation of IBRM.

Example Calculation

The BSM calculation for the adequate section shown in Fig. 2 (top) is summarized in Table 6 with a resultant BSM of 27 °F (−2.8 °C) falling in the adequate range. This process was repeated for the section with inadequate ballast (Fig. 2 (bottom)). Keeping all other parameters constant, the reduction in lateral strength for the inadequate section (i.e., 75 lbs/in (13.1 kN/m)) resulted in a BSM of 17 °F (−8.3 °C) which falls in the minimum required range (Table 2).

Results and Discussions

The buckle-risk methodology described in the earlier section was applied to 103 miles (166 km) of revenue service track on a Class I freight railroad. Both LR*AI*L and ATGMS data were collected and aligned, and the model was run on 327,673 individual crossties. The model results are presented at three distinct levels: subdivision, segment, and crosstie. At the subdivision level, results offer an overall indication of track health for a typical track subdivision (i.e., 100 miles (161 km)). The segment-level results provide a strip chart illustrating the specific parameters affecting track buckling and their associated buckle risk assessments for a much shorter length of track (i.e., 0.5-mi (0.8 km)). Finally, crosstie-level data are used to illustrate localized changes in track parameters over time, highlighting their direct impact on the BSM.

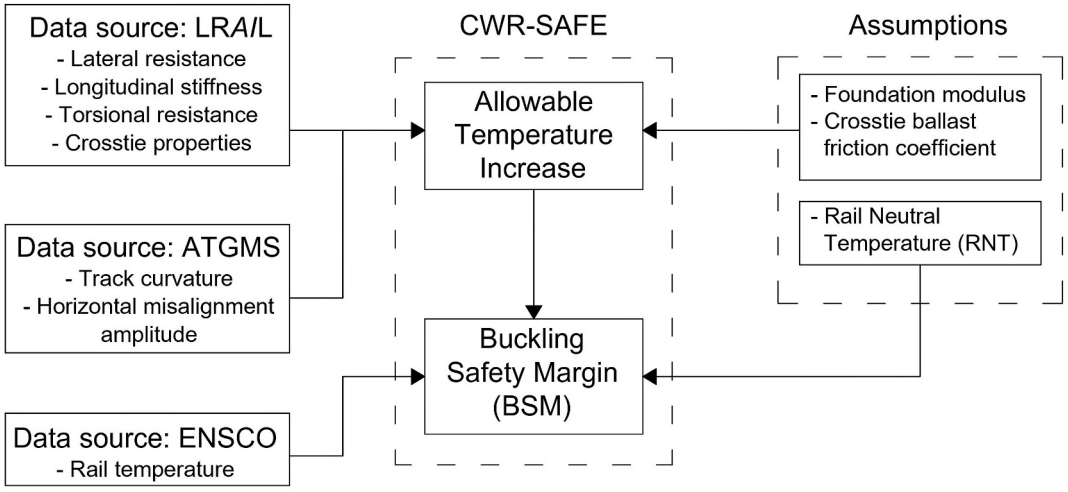

Fig. 3. Flowchart showing the data sources and assumptions made for calculation of allowable temperature increase and BSM using CWR-SAFE in the IBRM.

Table 6
BSM calculation example for an adequate section

Inputs Parameters	Value	Data Source/Remarks
Rail size	136 RE	Obtained from railroad inventory
Crosstie Type	Wood	LRAIL
Ballast type	Granite	
Crosstie lateral force (Peak resistance)	113 lbs/in (19.8 kN/m)	Calculated for adequate section
Crosstie weight	200 lbs (0.9 kN)	
Crosstie spacing	20 in (508 mm)	
Track curvature	4°	ATGMS
Crosstie ballast friction coefficient	1.2	Assumed for timber crosstie with granite ballast
Torsional resistance	80 in-kips/rad/in (356 m-kN/rad/m)	Cut spikes fastening system
Longitudinal stiffness	400 psi (2,758 kPa)	ETA anchorage pattern
Foundation modulus	3,000 psi (20.68 MPa)	Assumed for timber crosstie construction
Misalignment amplitude	in (2.54 mm)	ATGMS
Misalignment half – wavelength		Auto calculation by CWR-SAFE
Vehicle Type	Hopper	Most conservative (critical) rolling stock
Output Parameters	**Value**	**Data Source/Remarks**
Allowable Temperature Increase	87 °F (30.6 °C)	
Buckling Safety Margin (BSM)	27 °F (−2.8 °C)	BSM = $\Delta T_{allowable}$ – (T_{rail} – RNT) (Assuming T_{rail} = 140 °F and RNT = 80 °F)

Table 7
BSM results for a 103-mile (166-km) length of revenue service Class I track.

Range	BSM	Number of Crossties	Percentage of Total
Desired	> 40 °F (4.4 °C)	6,229	1.9 %
Adequate	20 to 40 °F (−6.7 to 4.4 °C)	313,521	95.7 %
Minimum Required	0 to 20 °F (−17.8 to −6.7 °C)	7,923	2.4 %

Subdivision Level

Results for 103 miles (166 km) of a Class I railroad primary corridor revealed that the majority of track was within the adequate BSM range (Table 7). However, 2.4 % of the total track length fell within the minimum BSM range, interspersed within sections of track with adequate buckle resistance. A 0.5-mile (0.8-km) track segment containing crossties within the minimum required BSM range is examined in greater detail in the subsequent section to identify the factors contributing to reduced BSM values.

Segment Level

A focused 0.5-mile (0.8-km) segment of the subdivision extending from Milepost (MP) 66.0 to 66.5 was chosen to demonstrate the results of the analysis in greater detail (Fig. 4). A strip chart was developed to present key parameters influencing BSM (Fig. 4). Presenting individual track parameters along the vertical axis while the MP is shown along the horizontal axis facilitates spatial visualization of parameter variation along the selected track segment. The upper section of the graphic displays the track layout, including degree of curvature, special track structures, and other physical infrastructure such as bridges and tunnels (Fig. 4). The example track segment has a 3°30′ right hand curve followed by a 4° left hand curve. Torsional resistance, representing the track's resistance to rotation in the horizontal plane is shown. In this track segment, all crossties are secured with cut spikes as indicated by the constant value of 80 in-kips/rad/in (356 m-kN/rad/m)[8]. The anchorage pattern of the crossties determines the longitudinal stiffness of the track. Most of the track segment has ETA anchorage pattern which corresponds to a longitudinal stiffness of 400 psi (2,758 kPa). However, locations near MP 66.0 and between MP 66.3 and 66.4 have EOTA thus a reduced longitudinal stiffness of 200 psi (1,379 kPa)[8].

The average horizontal misalignment values obtained from ATGMS are rounded up to the nearest 0.1 in. (2.5 mm) increment. Most of the track exhibits an average horizontal misalignment of approximately 0.1 in.. A notable increase in horizontal misalignment is observed near MP 66.4, which coincides with elevated lateral strength at the same location, potentially due to the recent addition of ballast. Variations in lateral strength along the track are attributed to inconsistent levels of shoulder and crib ballast. A noticeable reduction in ballast is evident between MP 66.4 and 66.5. The allowable temperature increase ($\Delta T_{allowable}$), a composite metric of the track's resistance to buckling, is adversely affected in this area. Specifically, the ballast deficiency has reduced $\Delta T_{allowable}$ to below 80 °F (26.7 °C) between MP 66.4 and 66.5, a track section located within a 4° curve.

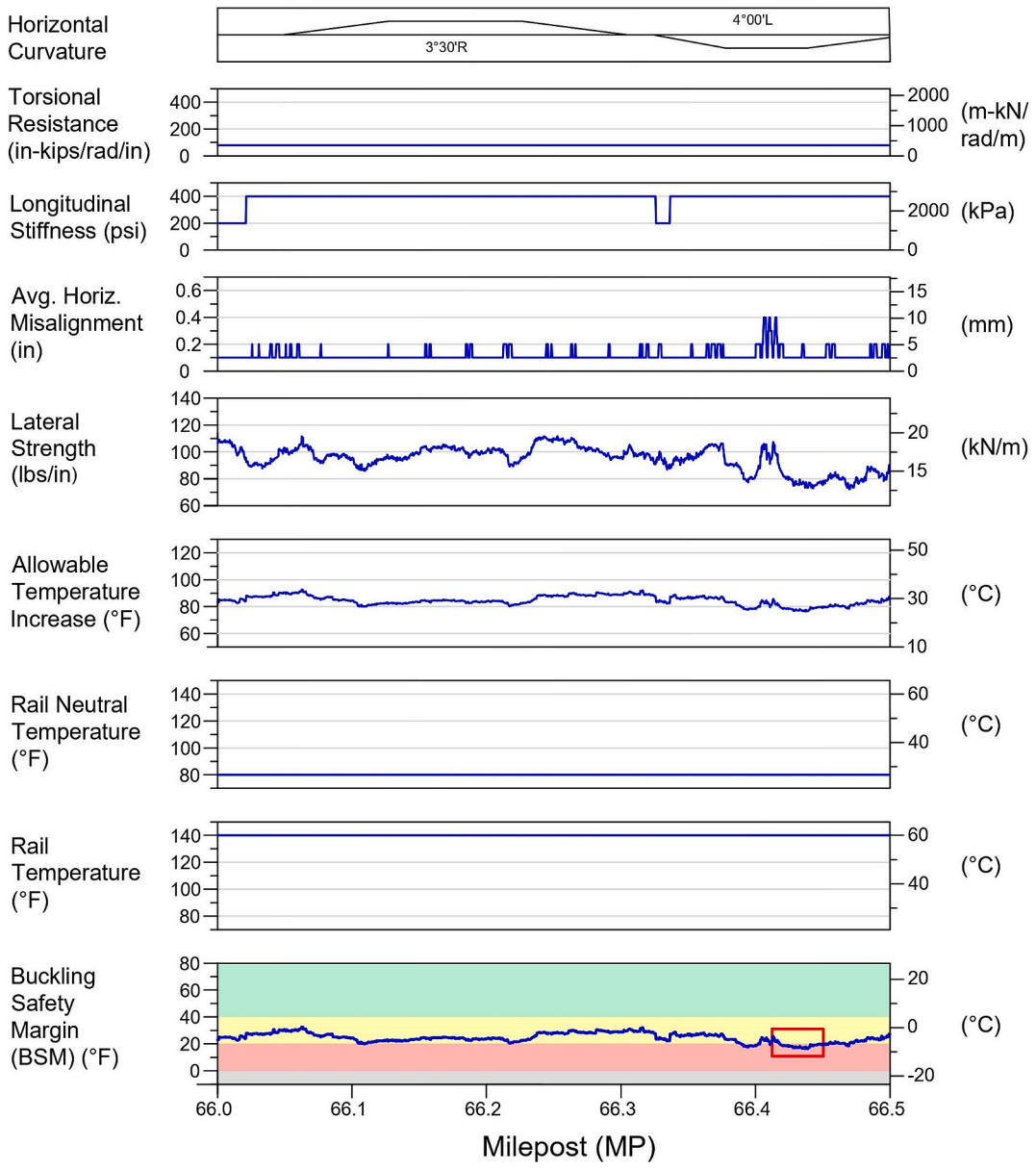

Fig. 4. Track chart showing track health parameters, allowable temperature increase, rail temperature, RNT, and BSM for a 0.5-mile (0.8-km) segment of revenue service Class I data.

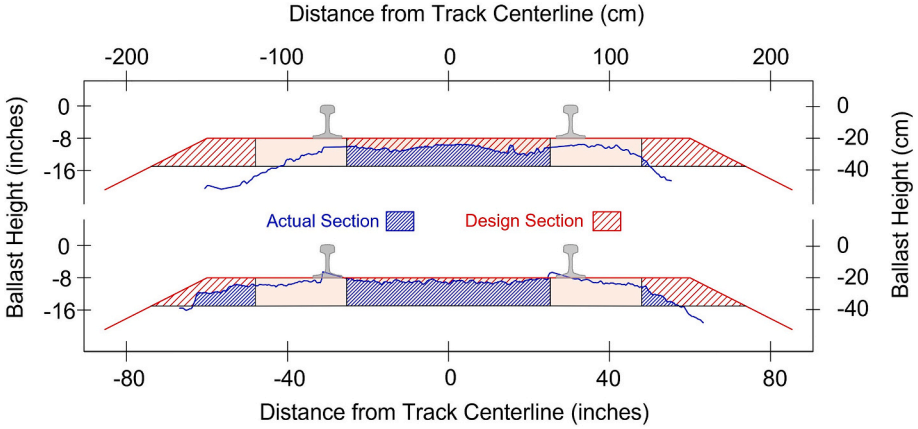

Fig. 5. Example showing changes to ballast cross-section properties at MP 66.42 between first (top) and second data collection runs (bottom).

The buckle-risk analysis presented in this study assumes a constant rail temperature of 140 °F and RNT of 80 °F across the entire corridor. Due to the additive linear relationship between the parameters influencing the BSM, a constant offset exists between $\Delta T_{allowable}$ and BSM (Equation (1)). For ease of interpretation, BSM ranges are color-coded (Table 2) in the background to aid in the identification of buckle-risk hotspots. As highlighted by the red box, the segment between MP 66.4 and 66.5 falls within the minimum required BSM range (< 20 °F) thus indicating a higher susceptibility to buckling.

Crosstie level

A crosstie at MP 66.42 has been plotted (Fig. 5) to show the condition of shoulder and crib ballast. A follow-up data collection run was conducted at the same location after an interval of eight months and accumulation of approximately 40 million gross tons (MGT) of freight traffic. The track parameters that changed over this period, along with their corresponding effects on the BSM, are summarized (Table 8). Notably, the lateral strength of the track improved between the two runs due to the addition of ballast. This enhancement contributed to an increase in the BSM; however, a portion of the strength gain was offset by an increase (i.e., doubling) in horizontal misalignment.

Discussion

The results obtained at the subdivision level highlight the effectiveness of the IBRM in identifying potential buckle hotspots over many miles of track. The segment-level data can aid railroad track maintenance personnel in planning maintenance interventions and identifying track parameters that need to be improved (i.e., strengthened) to reduce buckle risk. The quantification of key track parameters at a tie-by-tie resolution allows the model to perform a detailed assessment of buckle risk along the track. Additionally, it captures the impact of maintenance activities (e.g., ballast addition) on the BSM, thus demonstrating the model's ability to reflect changes in track condition over time. The results presented in this paper represent fully consolidated track. For tracks that have recently been tamped and thereby have partially-consolidated ballast, lower lateral strength values are applied. Furthermore, the model can also accommodate the influence of rail stress management practices by modifying the RNT for a specified segment of track. This capability supports the simulation of various track interventions and their effects on buckle risk, offering a valuable tool for determining both the timing and nature of appropriate maintenance activities.

A key strength of the IBRM lies in its flexibility. Localized track conditions, including the presence of fixed structures, can be simulated by adjusting parameters such as longitudinal stiffness and RNT. This adaptability supports the creation of a positive feedback loop, enabling iterative model refinement and improved predictive performance. Furthermore, the model can process subdivision-level data within a nominal computational timeframe, making it scalable for network-wide applications. It can efficiently handle large volumes of data from systems such as LRAIL and ATGMS, facilitating comprehensive and proactive track stability assessments across extensive rail networks.

Table 8
Summary comparison of results from crosstie at MP 66.42 between Run 1 and Run 2.

Track Parameters	First Run	Second Run
Crib Effectiveness	72 %	88 %
Shoulder Effectiveness	0 %	11 %
Total Peak Lateral Strength	75 lbs/in (13.1 kN/m)	87 lbs/in (15.2 kN/m)
Misalignment Amplitude	0.1 in. (2.54 mm)	0.2 in. (5.08 mm)
BSM	17 ℉ (−8.3 ℃) (Minimum Required)	20 ℉ (−6.7 ℃) (Adequate)

Conclusion and future work

Conclusion

Research has shown that track buckling is a complex phenomenon influenced by a wide range of track parameters. The emergence and adoption of modern railroad inspection technologies has enabled the collection of high-resolution track health data. Many U.S. Class I railroads have implemented ATGMS across large portions of their networks and are actively deploying 3D machine vision systems, or other combinations of systems that may provide similar data outputs (e.g., machine vision + LiDAR), along their primary corridors. The Illinois Buckle Risk Model (IBRM) has been developed as a data-driven tool that evaluates buckle risk through an experimentally-validated theoretical framework using data from modern track inspection systems.

IBRM was used to assess buckle risk by calculating the Buckling Safety Margin (BSM) for each crosstie in a Class I railroad subdivision. A strip chart illustrating all factors influencing buckle strength was developed, enabling rapid identification of stretches of track with low BSM values and clear visualization of the specific parameters contributing to reduced strength. Analysis of the subdivision data revealed that most of the track exhibited a BSM greater than 20 °F (−6.7 °C), while 2.4 % of the segment lengths fell within the minimum required range. These low-BSM segments should be prioritized for maintenance interventions. Furthermore, the predictive accuracy and effectiveness of IBRM can be enhanced by processing data from a larger portion of the network and at increased inspection frequencies. The model is also well-suited to evaluate track locations with known buckles, which can also be used to further validate and refine the model.

A recent comprehensive review of track buckling prediction methods by Agustin et al. [58] identified the development of buckle risk maps as a key research gap. The review proposed that maps be generated based on real-time track parameters and historical weather data to dynamically assess the likelihood of buckling events. The authors also emphasized the current lack of seamless integration between data sources and the limited ability of existing approaches to process and analyze real-time data at scale [58]. IBRM has the potential to address these research gaps due to its ability to efficiently process network-level data and integrate diverse data streams. Its scalability enables cost-effective buckle risk assessments, while its flexibility is demonstrated by its capacity to simulate localized track conditions. Therefore, IBRM is well-suited for the development of dynamic and data-driven buckle risk map.

Future Work

Despite the availability and use of high-resolution data for track components and geometry, localized values for rail temperature, RNT, and foundation modulus are presently unavailable. The IBRM applies a uniform rail temperature and RNT across the entire subdivision. Employing emerging data sources—such as rolling infrared measurements for rail temperature, detailed rail destressing records for RNT, and proxy measurements of foundation modulus—could further refine the model's accuracy. Although the current methodology evaluates track buckle risk on a tie-by-tie basis, previous research has shown that buckle lengths typically range from 30 to 50 ft (9–15 m)[8]. Consequently, it is essential to aggregate tie-by-tie outputs over track segments of appropriate length, ensuring that lateral strength, longitudinal stiffness, and torsional resistance are averaged or normalized accordingly. This approach captures the larger spatial scale of potential buckles more accurately. In addition, while this study employs a deterministic framework for model inputs, incorporating probabilistic distributions—particularly for RNT—would better account for uncertainties inherent in parameter estimation and further refine buckle risk assessment accuracy.

CRediT authorship contribution statement

Neeraj Thakur: Writing – original draft, Visualization, Methodology, Investigation, Formal analysis, Conceptualization. **Arthur de O. Lima:** Writing – review & editing, Supervision, Project administration, Methodology, Investigation, Funding acquisition, Data curation, Conceptualization. **Marcus S. Dersch:** Supervision, Project administration, Conceptualization. **J.Riley Edwards:** Writing – review & editing, Supervision, Project administration, Methodology, Investigation, Funding acquisition, Data curation, Conceptualization.

Declaration of competing interest

The authors declare that they have no known competing financial interests or personal relationships that could have appeared to influence the work reported in this paper.

Acknowledgments

This study was funded by the Federal Railroad Administration (FRA), part of the U.S. Department of Transportation (USDOT). The material in this paper represents the position of the authors and not necessarily that of its sponsors. Finally, the authors acknowledge the involvement and support from CSX and Union Pacific as Industry Partners.

Data availability

The data that has been used is confidential.

References

[1] Kerr, A.D. 1975. Lateral Buckling of Railroad Tracks due to Constrained Thermal Expansions — A Critical Survey, In: *Railroad Track Mechanics and Technology*. Pergamon. pp.141–169.
[2] Hauser D. *Methods for joining of Rails: Survey*. Report 1977;DOT-TSC-FRA-77-7.
[3] Sussmann T, Kish A, Trosino M. Influence of track maintenance on lateral resistance of concrete-tie track. Transportation Research Record 2003;1825(1): 56–63. https://doi.org/10.3141/1825-08.
[4] Wang, B.Z., C.P.L. Barkan and M. Rapik Saat. 2020. Quantitative Analysis of Changes in Freight Train Derailment Causes and Rates. *Journal of Transportation Engineering, Part A: Systems*, 146(11): 04020127 DOI: 10.1061/JTEPBS.0000453.
[5] FRA REA Database. 2025. Accident Data as reported by Railroads. URL https://safetydata.fra.dot.gov/OfficeofSafety/publicsite/on_the_fly_download.aspx. Accessed 2025-04-07.
[6] Kerr, A.D. 1976. *Analysis of Thermal Track Buckling in the Lateral Plane*. DOT-TSC-FRA-76-17.
[7] Samavedam G. Lateral Buckling of CWR Tracks. Journal of the Engineering Mechanics Division 1978;104(5):1284–8. https://doi.org/10.1061/JMCEA3.0002419.
[8] Kish, A. and G. Samavedam. 2013. *Track Buckling Prevention: Theory, Safety Concepts, and Applications*. DOT/FRA/ORD-13/16.
[9] Kish, A., G. Samavedam and D.Y. Jeong. 1985. *Influence of Vehicle Induced Loads on the Lateral Stability of CWR Track*. DOT-TSC-FRA-84-6.
[10] Samavedam, G., A. Kanaan, J. Pietrak, A. Kish and A. Sluz. 1995. *Wood Tie Track Resistance Characterization and Correlations Study*. DOT/FRA/ORD-94/07.
[11] Samavedam, G., A. Kish, A. Purple and J. Schoengart. 1993. *Parametric Analysis and Safety Concepts of CWR Track Buckling.* DOT-VNTSC-FRA-93-25.
[12] Allen, D.H. and D. Otter. 2018. *Improving Lateral Track Buckling Safety Margins*. MxV Rail, TD18-001. Pueblo, CO, USA.
[13] Esveld C. A better understanding of continuous welded rail track. Rail Engineering International 1996;25(4):13–6.
[14] Grissom GT, Kerr AD. Analysis of lateral track buckling using new frame-type equations. International Journal of Mechanical Sciences 2006;48(1):21–32. https://doi.org/10.1016/j.ijmecsci.2005.09.006.
[15] Kerr AD, Zarembski AM. On the new equations for the cross-tie track response in the lateral plane. Rail International 1986;17(6):13–21.
[16] Lim N-H, Park N-H, Kang Y-J. Stability of continuous welded rail track. Computers & Structures 2003;81(22):2219–36. https://doi.org/10.1016/S0045-7949(03)00287-6.
[17] Miura S. Lateral Track Stability: Theory and Practice in Japan. Transportation Research Record 1991;1289:53–63.
[18] Yang G, Bradford MA. Thermal-induced buckling and postbuckling analysis of continuous railway tracks. International Journal of Solids and Structures 2016; 97–98:637–49. https://doi.org/10.1016/j.ijsolstr.2016.04.037.
[19] Agustin D, Wu Q, Bernal E, Spiryagin M, Cole C. Railway track buckling evaluation using rigid-flexible multibody dynamic model and machine learning. Mech Based Des Struct Mach 2025;53(6):4830–52. https://doi.org/10.1080/15397734.2025.2456655.
[20] Agustin D, Wu Q, Spiryagin M, Cole C. A dynamic ballasted track model for buckling failure analysis. Eng Fail Anal 2025;170:109195. https://doi.org/10.1016/j.engfailanal.2024.109195.
[21] Kish A, Samavedam G, Jeong DY. *Analysis of thermal Buckling Tests on U.S.* Railroads 1982;DOT-TSC-FRA-82-6.
[22] Samavedam, G., A. Kish and D.Y. Jeong. 1986. *Experimental Investigations of Dynamic Buckling of CWR Tracks*. DOT-TSC-FRA-85-03.
[23] Kish A, Samavedam G. *Risk Analysis based CWR Track Buckling Safety evaluations*. Cambridge, MA, USA: US Department of Transportation's Volpe Center; 2001.
[24] Plaza, L. 2003. *Derailment of Amtrak Auto Train P052-18 on the CSXT Railroad Near Crescent City, Florida, April 18, 2002*. NTSB/RAR-03-02.
[25] Samavedam G, Blader F, Thomson D. *Safety of High speed Ground Transportation Systems, Track Lateral Shift: Fundamentals and State-Of-The-Art*. Review 1996. DOT/FRA/ORD-96/03.
[26] Zarembski AM, Grissom GT, Lees HM. Development of Track Buckling Risk Analysis Methodology. Nashville, TN, USA: The American Railway Engineering and Maintenance-of-Way Association; 2004.
[27] Huang C-L, Lee S, Popovics JS. Data-driven prediction of rail neutral temperature for continuously welded rails using impulse-based vibration frequencies. NDT & E International 2024;148:103229. https://doi.org/10.1016/j.ndteint.2024.103229.
[28] Kish, A. and G. Samavedam. 1987. Longitudinal Force Measurement in Continuous Welded Rail from Beam Column Deflection Response. American Railway Engineering Association (AREA), Washington, D.C., USA, pp. 280–301.
[29] Knopf K, Rizos DC, Qian Y, Sutton M. A non-contacting system for rail neutral temperature and stress measurements: Concept development. Structural Health Monitoring 2021;20(1):84–100. https://doi.org/10.1177/1475921720923116.
[30] Nucera C, Lanza di Scalea F. Nondestructive measurement of neutral temperature in continuous welded rails by nonlinear ultrasonic guided waves. The Journal of the Acoustical Society of America 2014;136(5):2561–74. https://doi.org/10.1121/1.4896463.
[31] Popovics, J.S., M.S. Dersch and X. Zhu. 2020. Vibration-based Longitudinal Rail Stress Estimation Exploiting Acoustic Measurement and Machine Learning - Rail Safety IDEA Program Project Final Report. *Transport Research Board of the National Academies*.
[32] Weaver, R.L. 2006. Vibration Measurement of Rail Stress - Final Report for High-speed Rail IDEA Project 48. *Transport Research Board of the National Academies*.
[33] Huang C-L, Wu Y, He X, Dersch M, Zhu X, Popovics JS. A review of non-destructive evaluation techniques for axial thermal stress and neutral temperature measurement in rail: Physical phenomena and performance assessment. NDT & E International 2023;137:102832. https://doi.org/10.1016/j.ndteint.2023.102832.
[34] Hay WW. *Railroad Engineering*. Second ed. New York, NY, USA: John Wiley & Sons; 1982.
[35] Federal Railroad Administration (FRA). 2011. Part 213 - Track Safety Standards, In: *Title 49 of the Code of Federal Registrations*. US Department of Transportation, Federal Railroad Administration, Washington, DC, USA. pp.100–154.
[36] Carr G, Tajaddini A, Nejikovsky B. Autonomous Track Inspection Systems - today and Tomorrow. Chicago, IL: The American Railway Engineering and Maintenance-of-Way Association Annual Meeting; 2009.
[37] Saadat S, Sherrock E, Zahaczewski J. *Autonomous Track Geometry Measurement Technology Design, Development.* and Testing; 2018.
[38] Saadat, S., C. Stuart, G. Carr and J. Payne. 2014. FRA Autonomous Track Geometry Measurement System Technology Development: Past, Present, and Future. In: *2014 Joint Rail Conference*, American Society of Mechanical Engineers, Colorado Springs, Colorado, USA, pp. V001T05A002.
[39] Morgado Bilheri T, Carvalho A. *Development of Relationships and Trending Methodologies for Railroad Track Component and Geometry Data.* Thesis: University of Illinois at Urbana-Champaign; 2023.
[40] Camargo LFM, Resendiz E, Hart J, Edwards JR, Ahuja N, Barkan CPL. *Machine Vision Inspection of Railroad Track*. NEXTRANS Project No 2011;0281Y02.
[41] Edwards JR, Hart JM, Sawadisavi S, Resendiz E, Barkan CPL, Ahuja N. *Advancements in railroad track inspection using machine-vision technology*. University of Illinois at 2009. Urbana-Champaign.
[42] Aytekin Ç, Rezaeitabar Y, Dogru S, Ulusoy İ. Railway Fastener Inspection by Real-Time Machine Vision. IEEE Transactions on Systems, Man, and Cybernetics: Systems 2015;45(7):1101–7. https://doi.org/10.1109/TSMC.2014.2388435.
[43] Circelli M, Kaviani N, Licciardello R, Ricci S, Rizzetto L, Arabani SS, et al. Track geometry monitoring by an on-board computer-vision-based sensor system. Transp Res Procedia 2023;69:257–64. https://doi.org/10.1016/j.trpro.2023.02.170.
[44] Guo, F., Y. Qian and Y. Shi. 2021. Real-time railroad track components inspection based on the improved YOLOv4 framework. *Automation in Construction*, 125: 103596 DOI: 10.1016/j.autcon.2021.103596.
[45] Aela P, Cai J, Jing G, Chi H-L. Vision-based monitoring of railway superstructure: a review. Constr Build Mater 2024;442:137385. https://doi.org/10.1016/j.conbuildmat.2024.137385.
[46] Wilk, S. and D. Li. 2023. *Relationship of Inspection Methods to Ballast Degradation Models: Phase I*. DOT/FRA/ORD-23/04.
[47] Asber J. *A Machine Learning-based Approach for Fault Detection of Railway Track and its Components*. Luleå, Sweden: Luleå University of Technology; 2020.
[48] Tulbure, A.-A., A.-A. Tulbure and E.-H. Dulf. 2022. A review on modern defect detection models using DCNNs – Deep convolutional neural networks. *Journal of Advanced Research*, 35: 33–48 DOI: 10.1016/j.jare.2021.03.015.
[49] Fox-Ivey, R., T.V. Nguyen, J. Laurent and Inc. Pavemetrics Systems. 2020b. *Laser Triangulation for Track Change and Defect Detection*. DOT/FRA/ORD-20/08.

[50] Fox-Ivey, R., T.V. Nguyen and J. Laurent. 2020a. *Extended Field Trials of LRAIL for Automated Track Change Detection*. DOT/FRA/ORD-20/14.
[51] .Harrington, R.M., A. de O. Lima, R. Fox-Ivey, T. Nguyen, J. Laurent, M.S. Dersch and J.R. Edwards. 2023. Use of deep convolutional neural networks and change detection technology for railway track inspections. *Proceedings of the Institution of Mechanical Engineers, Part F: Journal of Rail and Rapid Transit*, 237(2): 137–145 DOI: 10.1177/09544097221093486.
[52] Ramos, J.A.V.S., A. de O. Lima, M.S. Dersch and J.R. Edwards. 2025. Stochastic investigation of the relationship between track geometry and ballast degradation rates. *Transportation Geotechnics*, 51: 101533 DOI: 10.1016/j.trgeo.2025.101533.
[53] Bentley JL. Multidimensional binary search trees used for associative searching. Commun ACM 1975;18(9):509–17. https://doi.org/10.1145/361002.361007.
[54] Kish A. On the Fundamentals of Track Lateral Resistance. Minneapolis, MN: The American Railway Engineering and Maintenance-of-Way Association Annual Meeting; 2011.
[55] Al-Nazer, L. 2008. Development of Rail Temperature Prediction Model: Research Results. RR08-06.
[56] Kish A, Samavedam G. Improved Destressing of Continuous Welded Rail for Better Management of Rail Neutral Temperature. Transportation Research Record 2005; 1916(1):56–65. https://doi.org/10.1177/0361198105191600109.
[57] Kerr AD. *Fundamentals of Railway Track Engineering*. Omaha, NE, USA: Simmons Boardman; 2003.
[58] Agustin D, Wu Q, Ngamkhanong C. A review on railway track buckling prediction methods. Constr Build Mater 2025;466:140295. https://doi.org/10.1016/j.conbuildmat.2025.140295.